2010

The in-plane linear elastic constants and out-of-plane bending of 3-coordinated ligament and cylinder-ligament honeycombs.

Andrew Alderson
University of Bolton, A.Alderson@bolton.ac.uk

K. L. Alderson
University of Bolton, K.Alderson@bolton.ac.uk

G. Chirima
University of Bolton

N. Ravirala
University of Bolton

K.M. Zied
University of Bolton

The in-plane linear elastic constants and out-of-plane bending of 3-coordinated ligament and cylinder-ligament honeycombs

A. Alderson*, K. L. Alderson, G. Chirima, N. Ravirala and K. M. Zied

Centre for Materials Research and Innovation, University of Bolton, Deane Road, Bolton BL3 5AB, UK.

Abstract

Four novel cylinder-ligament honeycombs are described, where each cylinder has 3 tangentially-attached ligaments to form either a hexagonal or re-entrant hexagonal cellular network. The re-entrant cylinder-ligament honeycombs are reported for the first time. The in-plane linear elastic constants and out-of-plane bending response of these honeycombs are predicted using Finite Element (FE) modelling and comparison made with hexagonal and re-entrant hexagonal honeycombs without cylinders. A laser-crafted re-entrant cylinder-ligament honeycomb is manufactured and characterized to verify the FE model. The re-entrant honeycombs display negative Poisson's ratios and synclastic curvature upon out-of-plane bending. The hexagonal and 'trichiral' honeycombs possess positive Poisson's ratios and anticlastic curvature. The 'anti-trichiral' honeycomb (short ligament limit) displays negative Poisson's ratios when loaded in the plane of the honeycomb, but positive Poisson's ratio behaviour (anticlastic curvature) under out-of-plane bending. These responses are understood qualitatively through considering deformation occurs via direct ligament flexure and cylinder rotation-induced ligament flexure.

Keywords: A. Smart materials; B. Mechanical properties; C. Deformation; C. Elastic properties; C. Finite element analysis (FEA)

*** Corresponding author**: Tel: +44 (0)1204 903513; Fax: +44 (0)1204 399074; Email: A.Alderson@bolton.ac.uk

1. Introduction

Honeycombs combine light weight with good through-thickness strength and stiffness properties and find use as the core material in sandwich panel composites for aerospace, automotive and marine applications. The linear elastic properties of conventional hexagonal honeycombs (Figure 1a) are described well by analytical expressions [1] based on beam theory [2], and this understanding of structure-properties relationships has enabled the development of novel re-entrant hexagonal honeycombs (Figure 1b) displaying in-plane negative Poisson's ratio (auxetic [3]) response (e.g. [1,4,5].

Auxetic materials can have enhancements in other useful physical properties, including energy absorption, plane strain fracture toughness and the ability to form synclastic (dome shape) curvatures under out-of-plane bending [6]. Consequently, the potential to use auxetic honeycombs in advanced sandwich panel composites has provided the impetus to develop alternative auxetic honeycombs for optimal mechanical response. An alternative example of an auxetic honeycomb is the chiral cylinder-ligament honeycomb [7]. Cylinder-ligament honeycombs are attractive since the through-thickness shear response is enhanced by the ligaments [8] and the through-thickness compressive modulus and buckling are enhanced by the presence of the cylinders [9]. Hence it is possible to optimize the through-thickness behaviour through careful selection of the cylinder and ligament dimensions.

The first reported cylinder-ligament honeycomb comprised of an array of cylinders interconnected by ligaments: each ligament connecting two cylinders (located on opposite sides and ends of the ligament), with each cylinder having 6 ligaments tangentially attached to it at regular 60° intervals [7]. The system, therefore, has 6-fold chiral symmetry. More recently, alternative chiral connectivities have been reported, comprising cylinders having 3 or 4 tangentially-attached ligaments [10]. The 3-, 4- and 6- connected systems are termed trichiral, tetrachiral and hexachiral honeycombs,

respectively. Cylinder-ligament honeycombs in which adjacent cylinders are located on the same side of the interconnecting ligament have also been reported for 3- and 4-connectivities, known as anti-trichiral and anti-tetrachiral honeycombs, respectively [10]. The in-plane and through-thickness linear elastic properties of the 3-, 4- and 6-connected chiral and anti-chiral honeycombs have been reported [11,12]. The hexachiral, tetrachiral and anti-tetrachiral honeycombs are auxetic, but the trichiral honeycomb (Figure 1c) exhibits positive in-plane Poisson's ratios. The anti-trichiral honeycomb (Figure 1e) possesses positive Poisson's ratios in the long ligament limit, and undergoes a transition to negative Poisson's ratio response in the short ligament limit.

The 3-coordinated cylinder-ligament honeycombs are attractive from a light weight perspective since they contain fewer ligaments and cylinders than the 4- and 6-connected systems. In order to develop 3-coordinated systems with the added benefits associated with auxetic response, we report here for the first time two new 3-connected cylinder-ligament honeycombs based on the re-entrant hexagonal cell structure. The linear elastic in-plane and out-of-plane bending responses of these new honeycombs are compared with those of the existing trichiral and anti-trichiral honeycombs which are both based on a conventional hexagonal cell structure, and the conventional and re-entrant hexagonal honeycombs (i.e. the 3-coordinated systems in the limit of zero cylinder radius). The responses are considered in terms of the major deformation mechanisms acting in these honeycombs.

2. Honeycomb geometries

The 3-coordinated honeycombs are shown in Figure 1. The previously reported conventional hexagonal, re-entrant hexagonal, trichiral and anti-trichiral honeycombs are depicted in Figs. 1a, 1b, 1c and 1e, respectively. The new 3-connected cylinder-ligament honeycombs based on the re-entrant hexagonal cell structure are shown in

Figs. 1d and 1f, and are achieved by locating the tangentially attached ligaments at 60° intervals on each cylinder. The honeycomb containing cylinders located on opposite sides of the connecting ligament (Fig. 1d) is called the re-entrant trichiral system in recognition that the honeycomb is a hybrid of the trichiral and re-entrant hexagonal honeycombs. Similarly, the honeycomb containing cylinders connected on the same side of the connecting ligament (Fig. 1f) is called the re-entrant anti-trichiral system.

The off-axis ligaments have length L_1, the ligaments aligned along/towards the y axis have length L_2, the circular nodes have radius r, and the nodes and ligaments have common wall thickness t and depth d (Figure 1). Four dimensionless parameters are defined: $\alpha = L_1/r$, $\beta = t/r$, $\gamma = d/r$ [11] and $\delta = L_2/L_1$.

3. Finite Element model development

Simulations were performed using the ANSYS FE package, version 10.0.

3.1 In-plane mechanical properties

PLANE2 (linear elastic, solid) elements were employed in the simulations of the in-plane mechanical properties. Simulations were performed for small strains in the linear elastic region on arrays of several (typically 7×7 to 11×11) unit cells. x-directed forces were applied to the ligament nodes on the right-hand edge which were also constrained from displacement in the y direction. Nodes on the bottom and left-hand edges were constrained from in-plane rotation and translation normal to the edge direction, but were allowed to translate along the edge direction. This simulates the uniaxial test employed experimentally, and is shown for the trichiral honeycomb subject to tensile loading in Fig. 2a. The aspect ratio of the honeycomb in Fig. 2a could lead to the presence of Saint Venant effects in the simulations (for loading along x) but was chosen since it approximates the sample aspect ratio achievable experimentally. Forces in the y direction were applied to the ligament nodes on the top edge which were also

constrained from displacement in the x-direction. Nodes on the bottom and left-hand edges were constrained from in-plane rotation and translation normal to the edge direction, but were allowed to translate along the edge direction.

Strain in the *i* (= *x* or *y*) direction (ε_i) was calculated from the average relative displacement in the *i* direction of all pairs of ligament nodes on opposing edges having the same *j* (= *y* or *x*) coordinate, edge effects being minimized by the choice of suitably large arrays. Total stress (σ) was given by the sum of the nodal reaction forces on the edge to which compression was applied divided by the cross sectional area of the respective edge. The Poisson's ratios and Young's moduli were then calculated from the standard definitions: $\nu_{ij} = \frac{\varepsilon_j}{\varepsilon_i}$ and $E_i = \frac{\sigma_i}{\varepsilon_i}$, where *i* is the loading direction.

3.2 Out-of-plane bending

SHELL93 elements were employed in arrays of at least 7×5 unit cells in order to visualize the curvatures adopted by the honeycombs under out-of-plane bending. No mechanical property predictions were made in the out-of-plane bending simulations. Out-of-plane bending was simulated by constraining the nodes in the centre of each array from movement in all directions and applying a unit displacement normal to the plane to the central nodes of the two opposing edges aligned along the y direction. This is equivalent to bending of a honeycomb by hand at the edges, commonly used to demonstrate drapeability. Similar out-of-plane bending responses were obtained by applying a force rather than displacement to the edges. Figure 2b shows the loading conditions applied to the trichiral honeycomb, by way of example.

4. Analytical model for comparator conventional and re-entrant hexagonal honeycombs

Analytical expressions have been developed previously for the in-plane linear elastic properties of conventional and re-entrant hexagonal honeycombs assumed to deform by flexure of the ligaments [1] and also concurrent flexing, hinging and stretching of the ligaments [4,5]. The concurrent model has been found to give good agreement with FE simulations [5]. As an example, equation (1) is the expression for the in-plane Poisson's ratio for x direction loading of a hexagonal honeycomb deforming by concurrent flexing, hinging and stretching of the ligaments [4,5].

$$\nu_{xy} = \frac{\sin\theta\cos^2\theta\left(\frac{1}{K_f}+\frac{1}{K_h}-\frac{1}{K_s^{(L_1)}}\right)}{\left(\frac{L_2}{L_1}+\sin\theta\right)\left[\sin^2\theta\left(\frac{1}{K_f}+\frac{1}{K_h}\right)+\frac{\cos^2\theta}{K_s^{(L_1)}}\right]} \tag{1}$$

where the geometrical parameters are defined in Figure 1a. K_f, K_h and $K_s^{(L_1)}$ are force constants governing the flexing, hinging and stretching deformation mechanisms, respectively, and take the following forms [4,5]:

$$K_f = E_s b\left(\frac{t}{L_1}\right)^3 \tag{2a}$$

$$K_h = G_s b\left(\frac{t}{L_1}\right) = \frac{E_s b}{2(1+\nu_s)}\left(\frac{t}{L_1}\right) \tag{2b}$$

$$K_s^{(L_1)} = E_s b\left(\frac{t}{L_1}\right) \tag{2c}$$

where E_s, G_s and ν_s are the Young's modulus, shear modulus and Poisson's ratio of the ligament material which is assumed to be isotropic. From the definitions of α and β for the cylinder-ligament systems, we have:

$$\frac{\alpha}{\beta} = \left(\frac{L_1}{r}\right) \Big/ \left(\frac{t}{r}\right) = \frac{L_1}{t} \tag{3}$$

Substituting equations (2a)-(2c) and (3) into (1), and assuming $\nu_s = +0.25$, enables comparison of the hexagonal honeycombs with the cylinder-ligament honeycombs through the following relationship:

$$\nu_{xy} = \frac{\sin\theta\cos^2\theta\left(\left(\frac{\alpha}{\beta}\right)^2 + \frac{3}{2}\right)}{\left(\delta + \sin\theta\right)\left[\sin^2\theta\left(\left(\frac{\alpha}{\beta}\right)^2 + \frac{5}{2}\right) + \cos^2\theta\right]} \tag{4}$$

Similarly, the expression for E_x is adapted from [5]:

$$E_x = \frac{\beta E_s \cos\theta}{\alpha\left(\delta + \sin\theta\right)\left[\sin^2\theta\left(\left(\frac{\alpha}{\beta}\right)^2 + \frac{5}{2}\right) + \cos^2\theta\right]} \tag{5}$$

and equivalent expressions for ν_{yx} and E_y are also readily obtained from [5].

5. Experimental

5.1 Honeycomb fabrication

A laser-crafted re-entrant antitrichiral honeycomb was manufactured from an acrylic sheet (mechanical properties specified by manufacturer: $E_s = 2.5$GPa and $\nu_s = 0.25$) using a 40W laser crafting machine (World Lasers model: LR1612). The geometrical parameters of the test samples were $r = 3$mm, $L_1 = 15$mm, $L_2 = 30.5$mm, $t = 1.35$mm and $d = 2.1$mm (i.e. $\alpha = 5$, $\beta = 0.45$, $\gamma = 0.7$ and $\delta = 2.03$).

5.2 Mechanical properties characterisation

The honeycomb was tested in compression along the in-plane x direction in an Instron 4303 universal testing machine (25kN load cell and strain rate of 1mm/min), whilst simultaneously undertaking in-plane axial and transverse strain measurements from the movement of fiducial markers placed on the honeycomb using a MESSPHYSIK ME 46 videoextensometer. Figure 3 shows the test set-up for the sample (including fiducial markers). Several tests up to typically 1% applied strain were performed and the

average value of Poisson's ratio (ν_{xy}) and Young's modulus (E_x) evaluated from the slopes of the transverse strain vs axial strain and axial stress-strain curves, respectively.

6. Results

6.1 Poisson's ratios

Figure 4 shows transverse strain versus axial strain data for one compression test of the re-entrant antitrichiral honeycomb, clearly demonstrating this honeycomb displays auxetic behaviour. A Poisson's ratio of $\nu_{xy} = -0.775$ is determined from the negative of the slope of the least squares best fit line to the data, and an average over 5 compression tests yielded a value of $\nu_{xy} = -0.768 \pm 0.005$. This is in excellent agreement with the FE model prediction of $\nu_{xy} = -0.765$ – see Table 1.

The model Poisson's ratio predictions for all the honeycomb configurations considered in this paper are shown as a function of α in Figure 5. The predicted values for the trichiral and anti-trichiral honeycombs are consistent with those reported from FE models using a representative volume element (RVE) with periodic boundary conditions [11]: $\nu_{xy} = \nu_{yx}$ for both systems; the trichiral honeycomb displays positive Poisson's ratios for all values of α considered; and the anti-trichiral system undergoes a transition from positive (high α) to negative (low α) Poisson's ratio response. The re-entrant trichiral and re-entrant anti-trichiral systems, on the other hand, both display negative Poisson's ratios over all values of α considered. Further, for these latter systems $\nu_{xy} \neq \nu_{yx}$. For the re-entrant trichiral system $|\nu_{xy}| \sim |\nu_{yx}| + 0.1$ and both Poisson's ratios increase in magnitude with increasing α. In the case of the re-entrant anti-trichiral system, $|\nu_{yx}| > |\nu_{xy}|$ and the two Poisson's ratios tend towards convergence at large α. The analytical model Poisson's ratios of the conventional and re-entrant hexagonal honeycombs are insensitive to α: $\nu_{xy} = \nu_{yx} = +1$ and $\nu_{xy} = \nu_{yx} = -1$, respectively. The Poisson's ratios of the trichiral and anti-trichiral honeycombs tend to the conventional

hexagonal honeycomb values at high α, and those of the re-entrant trichiral and re-entrant anti-trichiral honeycombs tend to those of the re-entant hexagonal honeycomb at high α. Variation of β (ligament and cylinder wall thickness) was found to have little effect on the Poisson's ratios in the range $0.05<\beta<0.25$ considered in this paper.

6.2 Young's moduli

Figure 4 also includes stress-strain data (note the different plotting frequencies for the stress-strain and strain-strain data are due to different sampling rates of the universal testing machine and videoextensometer, respectively). The slope of the stress-strain data yields a Young's modulus for the test sample of E_x = 1.79MPa, and the average value from 8 tests was 1.78±0.08MPa. This is in good agreement with the value of E_x = 1.89MPa predicted from the FE model employing E_s = 2.50GPa (see Table 1).

The Young's moduli for all honeycombs are plotted as functions of α and β in Figures 6 and 7, respectively. The Young's moduli increase with decreasing α and increasing β. $E_x \sim E_y$ for the hexagonal, re-entrant hexagonal, trichiral and anti-trichiral systems. The curves for the hexagonal and re-entrant hexagonal honeycombs overlap, and these systems have the highest Young's moduli for any given value of α or β. The trichiral honeycomb displays higher Young's moduli than the antitrichiral honeycomb.

The re-entrant trichiral system also adheres reasonably well to $E_x \sim E_y$ (E_x is slightly higher than E_y), but not the re-entrant anti-trichiral system for which E_y is predicted to be higher than E_x (inserts in Figures 6 and 7). The re-entrant trichiral honeycomb has higher Young's moduli than the re-entrant anti-trichiral honeycomb E_x, but lower than the re-entrant anti-trichiral honeycomb E_y.

All the honeycombs studied are predicted to obey the condition of a symmetric compliance matrix ($\nu_{xy}E_y = \nu_{yx}E_x$).

6.3 Out-of-plane bending

The FE model simulations of honeycomb curvature when subject to out-of-plane bending deformation are shown for all honeycombs considered in this paper in Figure 8. The hexagonal and trichiral honeycombs possessing positive in-plane Poisson's ratios both undergo anticlastic (saddle-shape) curvature (Figs. 8a and 8c), whereas the negative in-plane Poisson's ratio re-entrant hexagonal, re-entrant trichiral and re-entrant anti-trichiral honeycombs adopt synclastic (dome-shape) curvature (Figs. 8b, 8e and 8f). Interestingly, the short ligament anti-trichiral honeycomb possesses negative in-plane Poisson's ratio response for in-plane loading ($\nu_{xy} \sim \nu_{yx} \sim -0.47$) yet is predicted to adopt anticlastic curvature (positive Poisson's ratio response) when subject to out-of-plane bending (Fig. 8d).

7. Discussion

The Poisson's ratios of the trichiral and anti-trichiral honeycombs tend towards those for the conventional hexagonal honeycomb at high α (Figure 5), reflecting the fact that in the long ligament limit, the trichiral and antitrichiral systems transform into the conventional hexagonal honeycomb (i.e. the cylinder node radius becomes negligible) [11]. Similarly, the re-entrant trichiral and re-entrant anti-trichiral honeycombs increasingly approximate the re-entrant hexagonal honeycomb as α increases, and so the Poisson's ratios for the re-entrant systems converge at high α.

The Young's moduli and Poisson's ratios predicted for the hexagonal and re-entrant hexagonal systems are consistent with previous studies on these honeycombs [1,4,5]. Similarly, the in-plane mechanical responses of the trichiral and anti-trichiral honeycombs predicted by the FE extended honeycomb array models employed in this work are consistent with the predictions from FE models using a RVE with periodic boundary conditions approach (with the exception that the RVE model predicts a transition from positive Poisson's ratio to negative Poisson's ratio as β decreases below

a critical value for the anti-trichiral honeycomb, whereas the extended array model predicts positive Poisson's ratios throughout) [11].

The in-plane linear elastic responses of the trichiral and anti-trichiral honeycombs have been explained previously through consideration of the deformation mechanisms predicted to occur in these systems [11]. The cylinder-ligament honeycombs deform predominantly by a combination of direct flexing of the ligaments, and flexing of the ligaments due to rotation of the cylinders in response to the applied load. In the trichiral system, direct flexing and cylinder rotation-induced flexing of the ligaments both lead to the same flexing mode (described as a 'full wave' deformed ligament shape [11]). For the anti-trichiral system, on the other hand, cylinder rotation induces a lower energy 'half wave' mode which, when combined with the full wave direct flexing mode, leads to lower Young's moduli for the anit-trichiral system with respect to the trichiral system for any given value of α or β (Figures 6 and 7). The full wave deformation mode produces positive Poisson's ratio behaviour for these systems, whereas the half wave deformation associated with cylinder rotation in the anti-trichiral honeycomb leads to auxetic behaviour. Hence, in the short ligament limit (low α), where cylinder rotation dominates the mechanical response, the anti-trichiral honeycomb is auxetic (Figure 5).

Consider, now, the re-entrant cylinder-ligament systems introduced in this work for the first time. For a tensile load applied in the x direction to the re-entrant anti-trichiral honeycomb (Figure 9), the off-axis (diagonal) ligaments experience direct flexure due to the applied load and undergo full wave flexural deformation. Flexure of ligaments in a re-entrant system is known to lead to auxetic behaviour [1]. A torque is also applied to each cylinder due to the applied external load, leading to rotation of the cylinders. For the re-entrant anti-trichiral system, connected cylinders rotate in opposite directions, and consequently the moments induced on the ligaments by the cylinders cause them to bend in a half wave manner. Pure half wave bending under tension

produces a lengthening of the cylinder-cylinder distance without changing the orientation of the connected cylinders with respect to each other. An increase in the cylinder-cylinder distance for those cylinders connected by off-axis ligaments leads to an increase in strain along the loading (x direction) but a decrease in strain along the transverse (y) direction. For those cylinders connected by ligaments aligned along the y direction, an increase in cylinder-cylinder distance leads to an increase in strain along y (to counteract the decrease in strain along this direction due to the off-axis ligaments) and no contribution to strain along the x direction. Consequently, the combined strain contributions due to cylinder rotation-induced half-wave flexure of off-axis and vertical ligaments lead to an increase in the total strain along x and only minor modification to the total strain along y. Similar arguments hold for a tensile load applied along the y direction, although in this case cylinder rotation is diminished due to the off-axis ligaments being under axial compression in a re-entrant system subject to tension along y and, therefore, applying a torque on each cylinder in opposition to that applied by the vertical ligaments (Figure 9). Consequently, the addition of cylinder rotation-induced strains to the direct ligament flexure strains leads to enhanced total strain along x and, therefore, $|\nu_{xy}|$ decreases and $|\nu_{yx}|$ increases with respect to the direct flexure-only (re-entrant hexagonal) honeycomb, particularly at low α where cylinder rotation effects are most pronounced (Figure 5). Similarly, the enhanced strain along x and the diminished role of the lower energy half-wave flexing mode for loading along y lead to $E_x < E_y$ for this system (Figures 6 and 7).

In the case of the re-entrant trichiral honeycomb under tensile loading along x, deformation modes include direct and cylinder rotation-induced flexing of the off-axis and ‘vertical’ (oriented almost parallel to y) ligaments (Figure 10 shows the deformation modes for loading along *x* by way of example). For the re-entrant trichiral honeycomb all cylinders rotate in the same direction and so cylinder rotation induces full wave flexing. The predicted Poisson’s ratio and Young’s moduli trends for the re-entrant

trichiral honeycomb can be explained using similar reasoning to that employed above for the re-entrant antitrichiral honeycomb. The mode of vertical rib flexure for the re-entrant trichiral honeycomb is not available to the re-entrant anti-trichiral honeycomb (vertical ribs are aligned parallel to the y axis) explaining why E_y (lower energy half-wave mode diminished) for the re-entrant anti-trichiral is greater than E_x for the re-entrant trichiral. The hexagonal and re-entrant hexagonal honeycombs display higher Young's moduli than the cylinder-ligament honeycombs for any given value of α or β. The additional deformation modes associated with the cylinders reduce the moduli in the cylinder-ligament systems compared to the non-cylinder containing honeycombs having fewer degrees of freedom.

Turning, now, to the out-of-plane bending responses (Figure 8). The predicted anticlastic and synclastic curvatures for the hexagonal (Figure 8a) and re-entrant hexagonal (Figure 8b) honeycombs, respectively, reproduce well the curvatures known for these systems [6] and expected from plate theory for positive and negative values of the in-plane Poisson's ratio, respectively [13]. The positive Poisson's ratio trichiral honeycomb undergoes the expected anticlastic curvature (Figure 8c), and the auxetic re-entrant trichiral (Figure 8e) and re-entrant anit-trichiral (Figure 8f) honeycombs display the expected synclastic curvature.

However, interestingly, the short ligament limit anti-trichiral honeycomb possessing negative in-plane Poisson's ratios is predicted to exhibit anticlastic curvature expected for positive Poisson's ratio honeycombs when bent out of plane (Figure 8d). The explanation lies in consideration of the deformation mechanisms identified previously for this honeycomb [11]. The auxetic behaviour arises due to cylinder rotation-induced half wave flexing of the ligaments which, in the short ligament limit, dominates the concurrent non-auxetic direct full wave flexing of the ligaments. When subject to out-of-plane bending deformation the top surface of the honeycomb is placed under axial tension and the bottom surface under axial compression. Hence the torque

applied to each cylinder on the top surface opposes the torque applied on the bottom surface, leading to a cancellation of the cylinder rotation mechanism responsible for the auxetic response. Since the cylinder rotation mechanism is, then, redundant for out-of-plane bending, the in-plane Poisson's ratio of the system will tend towards that given by equation (4) (i.e. $\nu_{xy} = \nu_{yx} \rightarrow +1$) and hence the predicted anticlastic curvature. The anti-trichiral honeycomb is an example of a material/structure which possesses negative Poisson's ratio response when subject to in-plane deformation, but positive Poisson's ratio response when subject to out-of-plane bending. A composite 3-ply laminate displaying this unusual mechanical response has also been recently reported [14].

The results presented in this paper extend the range of cylinder-ligament honeycombs, and include the development of the first hybrid re-entrant hexagonal cylinder-ligament systems. As such, the range of alternative honeycomb geometries to the commonly used conventional hexagon is expanded, and the ability to tailor the mechanical response due to the new geometries has been demonstrated (including auxetic response). The model results for a hybrid system have been validated against experimental data in this paper. FE model data for the trichiral and antitrichiral systems are in good agreement with single-cell periodic boundary condition FE model data presented and validated against experimental data in a companion paper [11], demonstrating the robustness of the results. Auxetic honeycombs have significance since they lead to the potential to produce curved structures for use in sandwich panels for aerospace, automotive and marine applications. The cylinder-ligament architecture provides means to enhance and optimize through-thickness compression (cylinder) [9] and shear (ligament) [8] response, and also provides a host structure for embedded sensor and actuator elements for structural health monitoring and other smart/active materials applications.

8. Conclusions

The linear elastic responses of hexagonal, re-entrant hexagonal, trichiral, anti-trichiral, re-entrant trichiral and re-entrant anti-trichiral honeycombs subject to in-plane uniaxial and out-of-plane bending loading have been investigated using an FE model extended array approach. The re-entrant trichiral and re-entrant anti-trichiral honeycombs have been introduced for the first time, and are hybrids of the re-entrant hexagonal honeycomb with the trichiral and anti-trichiral honeycombs, respectively. Experimental testing of a re-entrant anti-trichiral has been used to verify the FE model. The predicted in-plane linear elastic responses of the hexagonal, re-entrant hexagonal, trichiral and anti-trichiral honeycombs agree with previous studies. The new re-entrant trichiral and re-entrant anti-trichiral honeycombs both display in-plane negative Poisson's ratios. Anticlastic curvature is predicted for the positive Poisson's ratio hexagonal and trichiral honeycombs, and synclastic curvature is predicted for the negative Poisson's ratio re-entrant hexagonal, re-entrant trichiral and re-entrant anti-trichiral honeycombs. The anit-trichiral honeycomb displays negative Poisson's ratios under uniaxial in-plane loading and positive Poisson's ratio response for out-of-plane bending. Qualitative understanding of the Poisson's ratios, Young's moduli and out-of-plane bending curvatures has been developed based on the main deformation mechanisms acting in these systems: direct flexing and cylinder rotation-induced flexing of ligaments.

Acknowledgements. This work has been performed as part of the European Union 6th Framework Programme STREP project NMP3-CT-2005-013641 - CHISMACOMB.

References

1. Gibson LJ, Ashby MF. Cellular solids, Structure and Properties. Cambridge University Press, Cambridge, second edition, 1997.

2. Timoshenko SP. Strength of Materials Part 1, Elementary Theory and Problems. Van Nostrand, New York, third edition, 1955.

3. Evans KE, Nkansah MA, Hutchinson IJ, Rogers SC. Molecular Network Design, Nature 1991;353:124.

4. Masters IG, Evans KE. Models for the elastic deformation of honeycombs. Compos. Struct. 1997;35:403-422.

5. Whitty JPM, Nazare F, Alderson A. Modelling the effects of density variations on the in-plane Poisson's ratios and Young's moduli of periodic conventional and re-entrant honeycombs - Part 1: Rib thickness variations. Cellular Polymers 2002;21(2):69-98.

6. Alderson A, Alderson KL. Auxetic Materials. Proc. Inst. Mech. Eng., Part G, J. Aero. Eng. 2007;221:565-575.

7. Prall D, Lakes R. Properties of a chiral honeycomb with Poisson's ratio –1. Int. J. Mech. Sci. 1996;39:305-314.

8. Lew TL, Spadoni A, Scarpa F, Ruzzene M. Chiral hexagonal cellular sandwich structure: A vibroacoustic assessment. Proceedings of SPIE 2005;5760:559-568.

9. Spadoni A, Ruzzene M, Scarpa F. Global and local linear buckling behaviour of a chiral cellular structure. Physica Status Solidi (b) 2005;242(3):695–709.

10. Grima JN. New Auxetic Materials, PhD thesis, Exeter University, 2000.

11. Alderson A, Alderson KL, Attard D, Evans KE, Gatt R, Grima JN, Miller W, Ravirala N, Smith CW, Zied K. Elastic constants of 3-, 4- and 6- connected chiral and

antichiral honeycombs subject to uniaxial in-plane loading. Comp. Sci. Tech. 2008: submitted.

12. Lorato A, Innocenti P, Scarpa F, Alderson A, Alderson KL, Zied KM, Ravirala N, Miller W, Smith CW, Evans KE. The transverse elastic properties of chiral honeycombs. Comp. Sci. Tech. 2008: submitted.

13. Evans KE. Design of doubly-curved sandwich panels with honeycomb cores. Compos. Struct. 1990;17:95-111.

14. Lim T-C. On simultaneous positive and negative Poisson's ratio laminates. Phys. Stat. Sol. B. 2007;244(3):910-918.

FIGURES

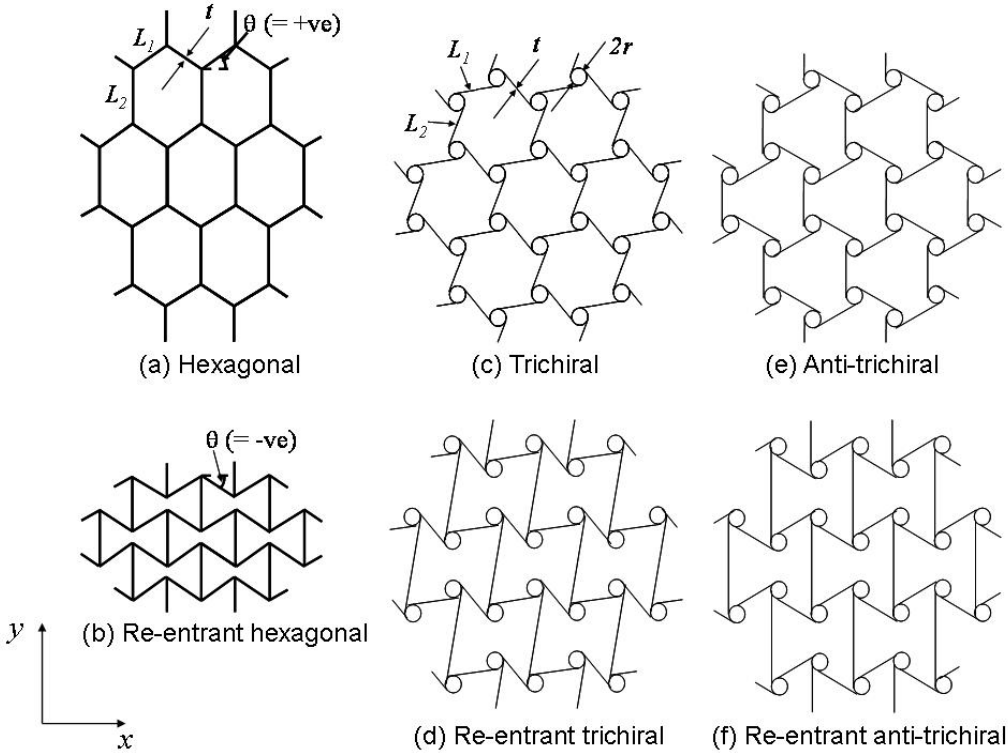

Fig. 1 Honeycombs investigated in this study: (a) Hexagonal; (b) Re-entrant hexagonal; (c) Trichiral; (d) Re-entrant trichiral; (e) Anti-trichiral; (f) Re-entrant anti-trichiral.

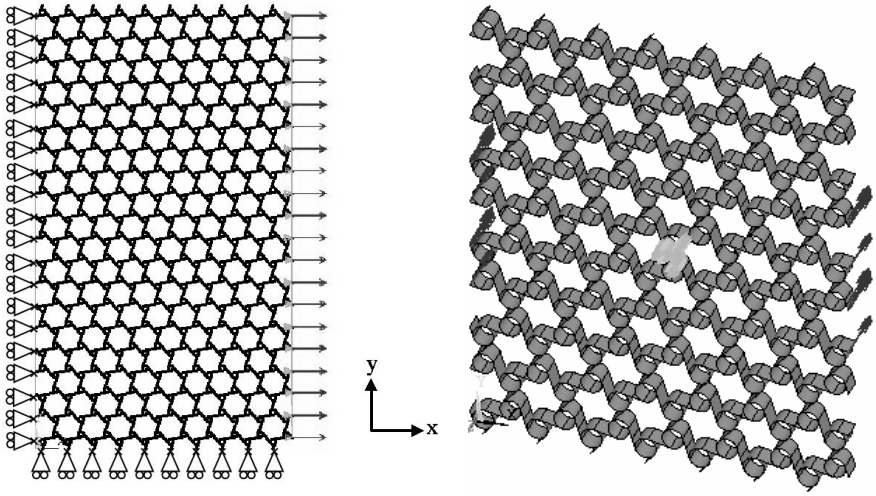

Fig. 2 Loading and boundary conditions for the trichiral honeycomb undergoing (a) in-plane uniaxial tension along x and (b) out-of-plane bending.

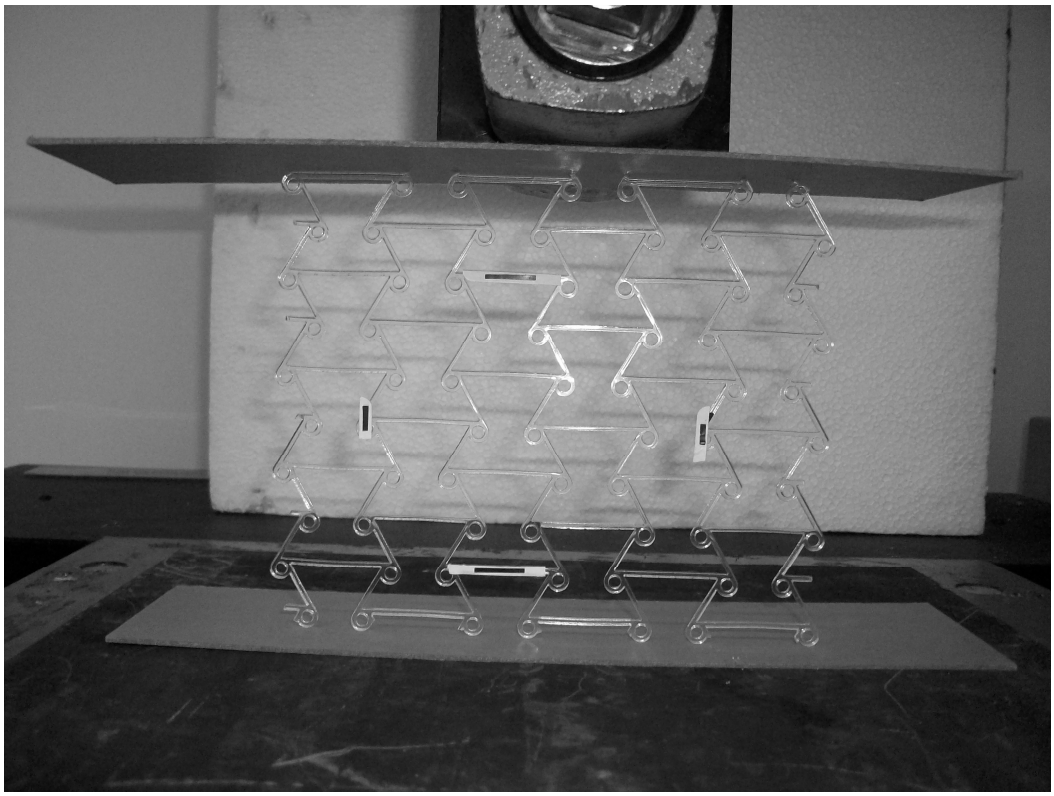

Fig. 3 Uniaxial compression (along x) of the re-entrant anti-trichiral honeycomb, with fiducial markers attached for videoextensometer measurement.

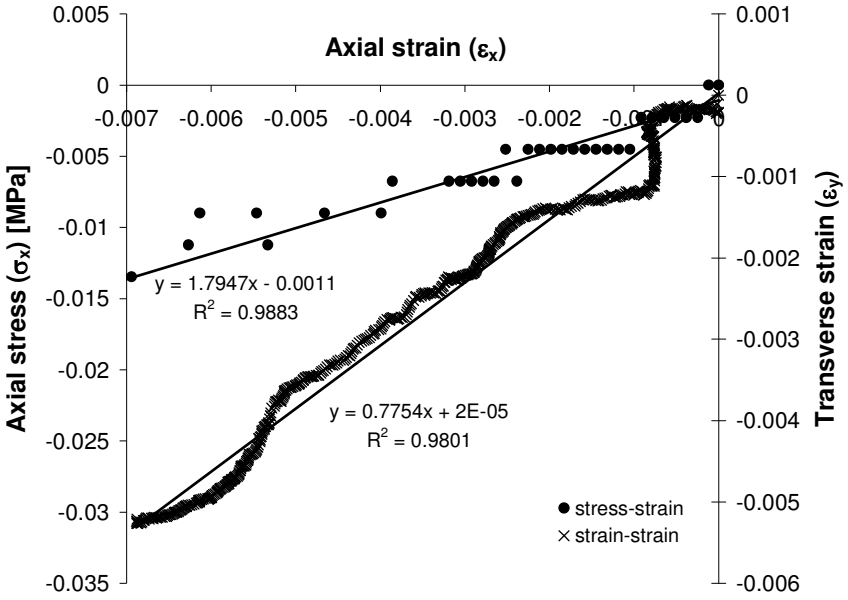

Fig. 4 Experimental stress-strain (circles) and strain-strain (crosses) data for the re-entrant anti-trichiral honeycomb under uniaxial compression.

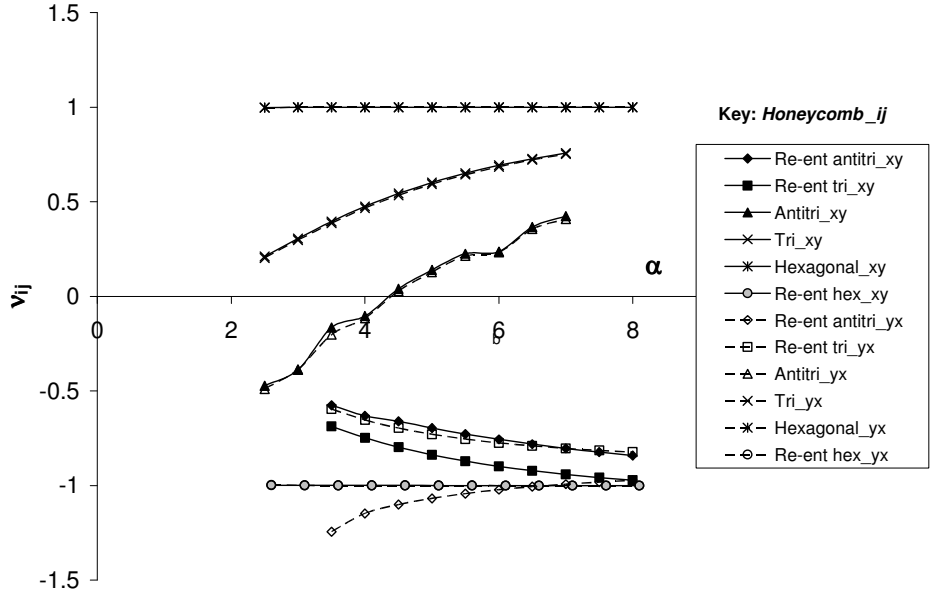

Fig. 5 Model predictions for Poisson's ratio (ν_{xy} = filled symbols and solid lines; ν_{yx} = empty symbols and dashed lines) as a function of α for the re-entrant anti-trichiral (diamond), re-entrant trichiral (squares), anti-trichiral (triangles), trichiral (crosses), hexagonal (stars) and re-entrant hexagonal (circles) honeycombs. $\beta = 0.05$ and $\gamma = 5$ for all cases; $\delta = 2$ for the re-entrant systems, and $\delta = 1$ for all other systems.

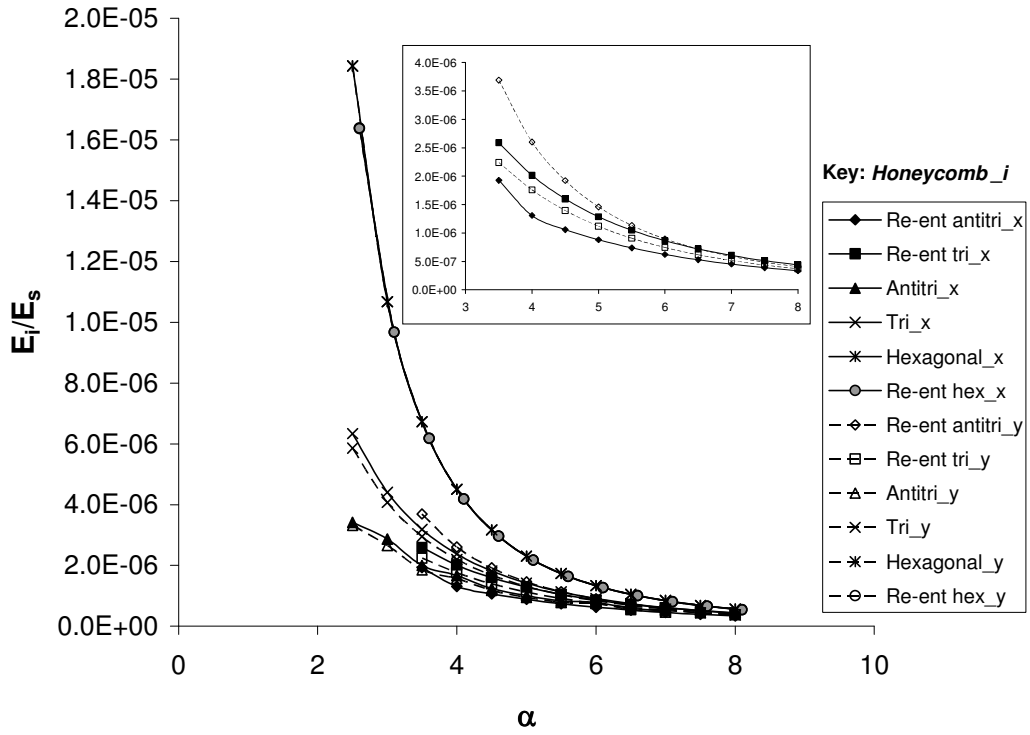

Fig. 6 Model predictions for Young's modulus (E/E_s) vs α. Symbols as for Fig. 5. β = 0.05 and γ = 5 for all cases; δ = 2 for the re-entrant systems, δ = 1 for all other systems.

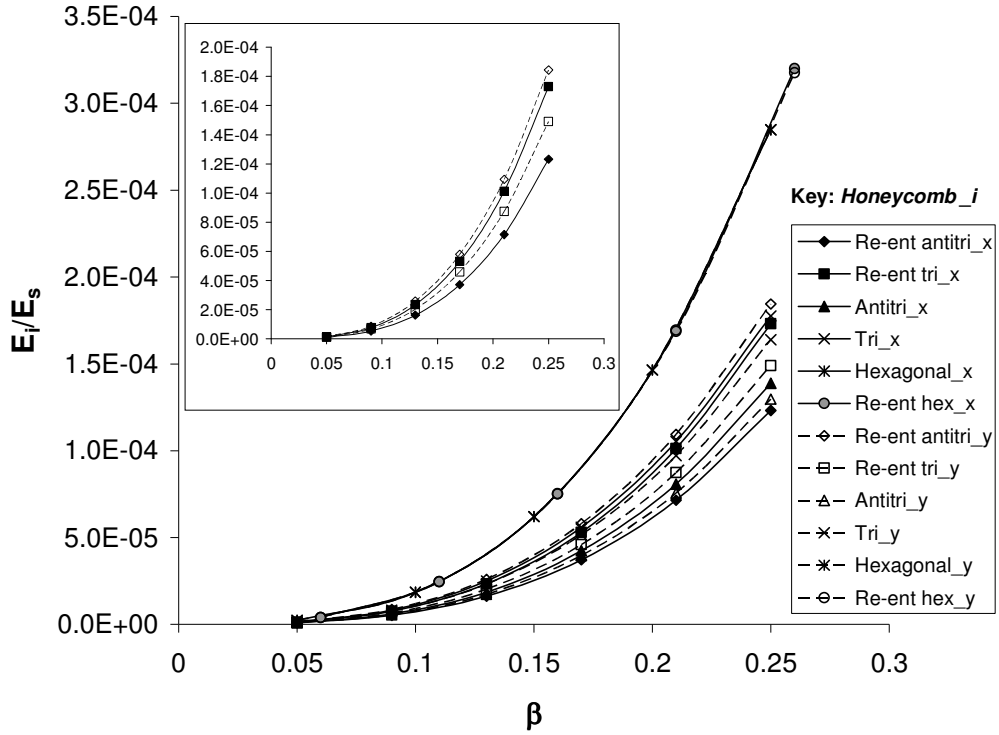

Fig. 7 Model predictions for Young's modulus (E/E_s) as a function of β. Symbols as for Fig. 5. α = γ = 5 in all cases; δ = 2 for the re-entrant systems, δ = 1 for all other systems.

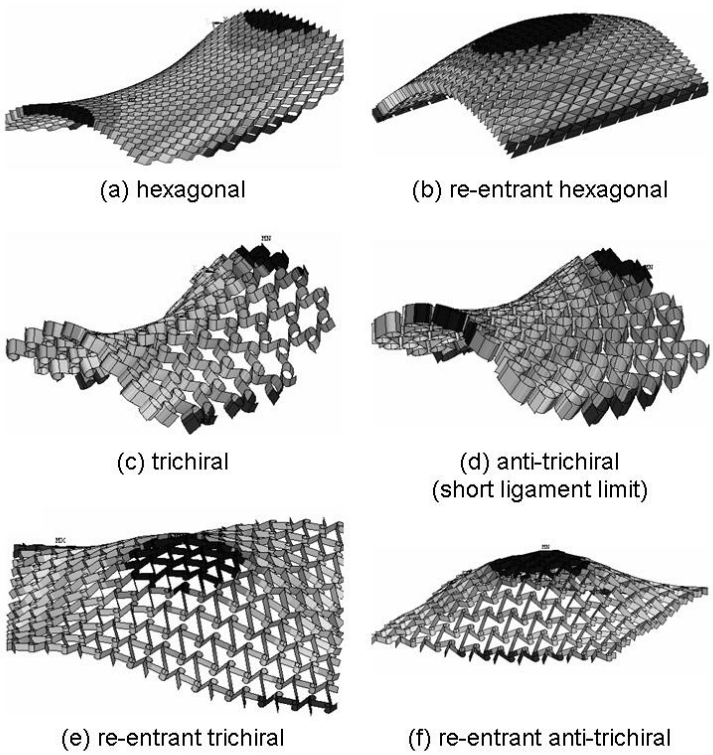

Fig. 8 FE model out-of-plane bending predictions for (a) hexagonal (positive in-plane ν), (b) re-entrant hexagonal (negative in-plane ν), (c) trichiral (positive in-plane ν), (d) short ligament anti-trichiral (negative in-plane ν), (e) re-entrant trichiral (negative in-plane ν) and (f) re-entrant anti-trichiral (negative in-plane ν) honeycombs. Shading corresponds to z-direction displacement.

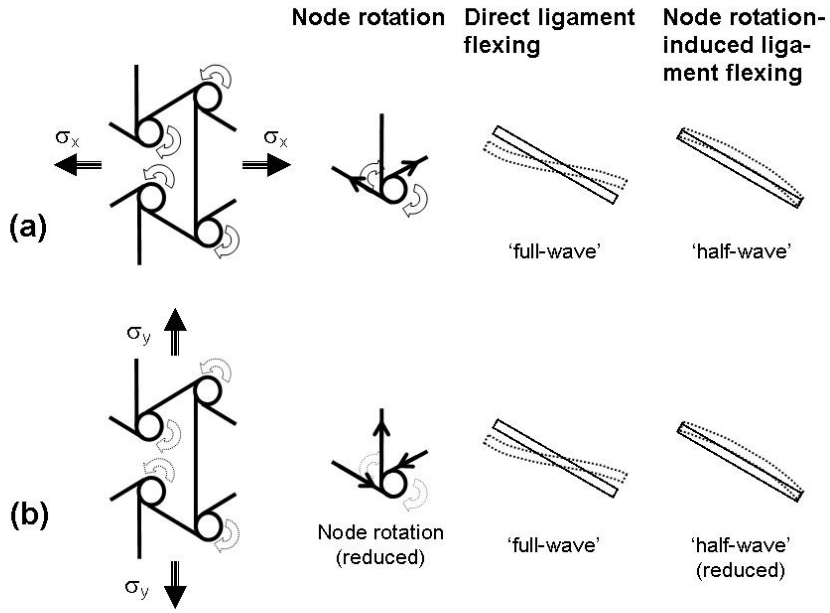

Fig. 9 Deformation mechanisms in the re-entrant anti-trichiral honeycomb under (a) loading along *x* and (b) loading along *y*.

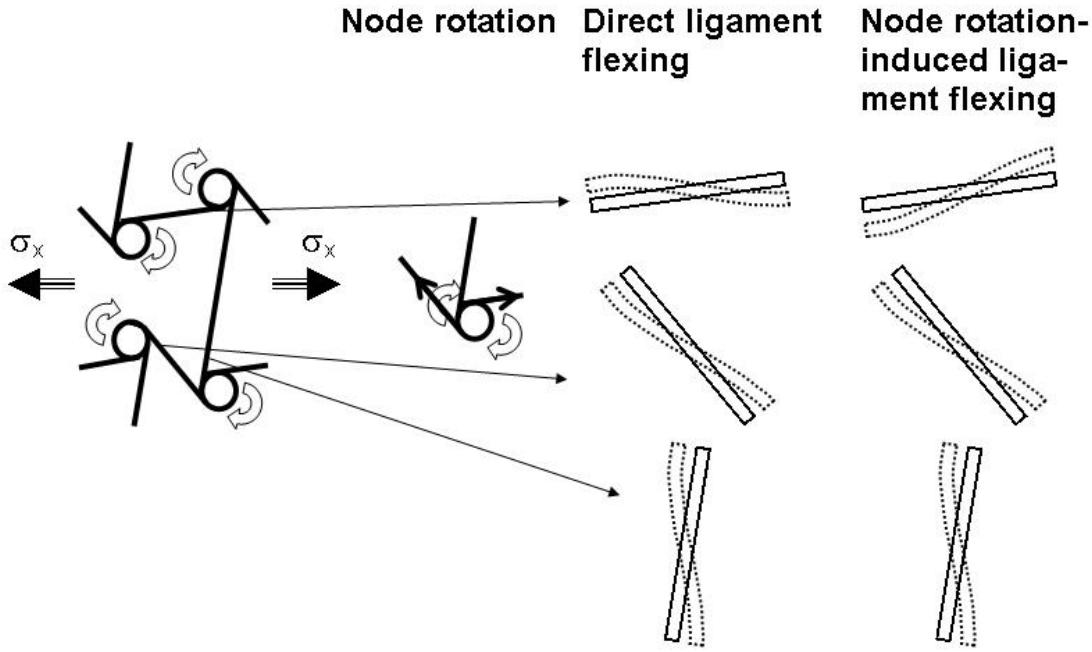

Fig. 10 Deformation mechanisms in the re-entrant trichiral honeycomb under loading along *x*.

Table 1: Experimental and FE model in-plane elastic constants (Young's moduli and Poisson's ratios) for the re-entrant antitrichiral honeycomb.

	ν_{xy}	E_x (MPa)
Experiment	-0.768±0.005	1.78±0.08
FE model	-0.765	1.89